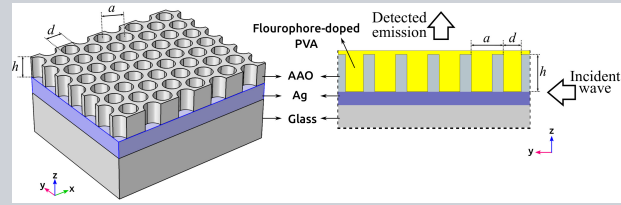


**Abstract** A class of hybrid photonic-plasmonic structures (HPPS) with vertical cylindrical cavities is proposed, which enables one adjusting hybrid photonic-plasmonic optical modes to obtain coherence for spontaneous emission of different fluorescent molecules. The thorough and efficient analysis of the emission of a large number of fluorophores in the presence of HPPS is merely possible using the proposed numerical method, in which an innovative semi-classical algorithm is implemented to capture the statistical nature of the problem. This is in contrast to the deterministic approach that was conventionally adopted for time-domain methods. In this paper, it is shown that the proposed easy-to-fabricate and robust anodic aluminum oxide structure dramatically enhances the temporal and spatial coherence compared to the previously examined HPPS.



## Fluorescence coherence with anodic aluminum oxide hybrid photonic-plasmonic structure: numerical analysis using an innovative statistical approach

Ali Reza Hashemi and Mahmood Hosseini-Farzad\*

Fluorescence is a vastly used optical method for chemical and biological detection [1, 2]; however, its performance and efficiency shall be enhanced especially in sensing and imaging applications [3–6]. Plasmonics appears to be the best method for tailoring and enhancing the fluorescence emission [7]. It is known that light can be confined in close vicinity of metallic surfaces or nano-particles due to the coupling between electromagnetic (EM) waves and oscillations of electrical charges at the surface. The idea is to employ this interaction, which is referred to as surface plasmon resonance (SPR) in a way that a large enhancement in the optical density of states can be obtained in the neighborhood of fluorophores. This will be an effective means for elevating the excitation rate and raising the quantum yield as well as controlling the angular distribution of the fluorescence emission [8–12].

Although the presence of fluorophore in the vicinity of metallic structures leads to the above mentioned appealing features, this adjacency may also increase the probability of quenching and non-radiative energy loss for the excited fluorophore [13–16]. This inadequacy can be resolved by means of a hybrid photonic-plasmonic structure (HPPS), that is created by attaching a photonic crystal (PC) to the metal surface (plasmonic structure). In other words, coupling between the surface plasmon polaritons (SPPs), i.e. the EM waves which are confined along the metal-dielectric interface, and the guided or trapped modes of the photonic crystal leads to the striking features of increasing the propagation length of SPPs, confining light in a deep subwavelength

scale, and highly guided modes and cavity resonances in the PC structure [17–20]. Moreover, by using an HPPS, the effective length of the evanescent normal component of SPPs can extend to tens of nanometers above the metal surface, therefore, the enhancement and directionality are obtained without any significant quenching [21–23].

On the other hand, due to the weak correlation between the spontaneous emissions of fluorophores, the resulted light is isotropic in space and broad in spectrum, which in turn lowers the detectability. Therefore, it is potentially advantageous to utilize a technique to create a coherent light from such spontaneous emitters. It must be noted that a desirable technique shall also prevent any significant loss in the emission intensity [24–26]. Such a technique can play an important role in different fluorescence applications. Recently, special HPPSs have been proposed, for which a partially coherent light is obtained from fluorescence emission [27, 28]; nevertheless, the adaptability of these structures to different spontaneous emitters has not yet been addressed.

The aim of the present work is to propose a robust and easy to fabricate HPPS, which substantially enhances such coherence, while brings the required flexibility to be adjusted for spontaneous emitters with different excitation/emission frequencies. Nevertheless, this requires investigating the fluorescence emission near plasmonic nanostructures, which is still an open area for researches [3]. Considering the practical limitations of the delicate experimental setups, a rather low-cost numerical method can be effectively employed to provide guidelines for experi-

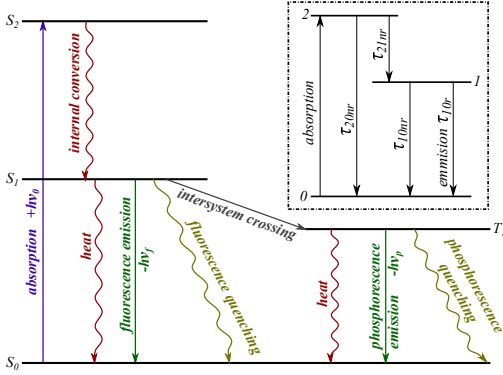


**Figure 1** Jablonski diagram showing electronic transitions of a molecule with radiative and non-radiative transitions from/to singlet ( $S$ ) and triplet ( $T$ ) states. The simplified model for a fluorescent molecule is shown in the inset.

ments [29, 30] while it also advances our fundamental understanding of physical phenomena [31–34].

The conventional implementation of fluorescence in numerical methods is based on representing the molecular dipole moment of fluorophores by using a damped driven harmonic oscillator differential equation [35–37]. Nonetheless, this technique is incapable of making any distinction between the excitation and emission frequency of the molecules. More importantly, using a single deterministic equation in the numerical simulations, it is impossible to attribute statistical characteristics, e.g. coherence, to an ensemble of fluorophores. In this work, a novel algorithm is proposed to resolve this issue by introducing the probabilistic nature of the molecular transitions into the numerical method. This algorithm is implemented within the framework of finite-difference time-domain (FDTD) method [38] and validated against previously reported experimental results.

Energy bands of a single fluorescent molecule can be modeled as a three (energy) level system, for which absorption and both radiative and non-radiative transitions occur [39, 40] (Fig. 1). The probabilities associated with possible transitions are estimated as follows.

**Absorption:** For the electric dipole moment of a fluorophore  $\mathbf{p}$  with maximum absorption frequency  $\omega_a$ , a forced harmonic oscillator differential equation is considered as

$$\ddot{\mathbf{p}} + \omega_a^2 \mathbf{p} = (e^2/m_e) \mathbf{E}(t), \quad (1)$$

where  $e$  and  $m_e$  are the charge and mass of electron, respectively. In this equation,  $\mathbf{E}(t)$  is the electric field imposed at the position of molecule. The resonance of  $\mathbf{p}$  leads to the absorption of energy  $\mathbf{E} \cdot \mathbf{p}$  via the Ampere-Maxwell's relation  $\epsilon \dot{\mathbf{E}} = \nabla \times \mathbf{H} - \dot{\mathbf{p}}$  and the probability of transition from level 0 to level 2 is

$$P_{02}(t) = \exp\left(-(\hbar\omega_a - \mathbf{E}(t) \cdot \mathbf{p}(t))^2 / \sigma_a^2\right), \quad (2)$$

where  $\sigma_a$  corresponds to the excitation bandwidth of fluorophore.

**Non-radiative transitions:** For the present model, three non-radiative transitions are considered;  $2 \xrightarrow{nr} 1$ ,  $2 \xrightarrow{nr} 0$  and  $1 \xrightarrow{nr} 0$ . The corresponding probabilities are estimated as

$$P_{21nr}(t) = A \left(1 - \exp\left(-\frac{t}{\tau_{21nr}}\right)\right) \quad (3)$$

$$P_{20nr}(t) = B \left(1 - \exp\left(-\frac{t}{\tau_{20nr}}\right)\right) \quad (4)$$

$$P_{10nr}(t) = C \left(1 - \exp\left(-\frac{t}{\tau_{10nr}}\right)\right) \quad (5)$$

Here,  $\tau_{ijnr}$  represents the time-constant for a non-radiative decay between levels  $i$  and  $j$ . The asymptotic behavior of these functions guaranties a definite decay at an infinitely long time.

**Radiative transition:** Radiative transition is only considered as a decay from level 1 to level 0, for which the corresponding probability is estimated as

$$P_{10r}(t) = D \left(1 - \exp\left(-\frac{t}{\tau_{10r}}\right)\right), \quad (6)$$

where  $\tau_{10r}$  is the time constant of the radiative decay. Once the transition occurs, a wave packet with the central frequency equal to emission frequency of the fluorophore  $\omega_e$  is emitted from a point source at the position of the molecule.

The normalization factors  $A, B, C, D$  are calculated based on two physical concepts; it is impossible for a molecule to permanently stay at an excited state ( $A + B = 1$  and  $C + D = 1$ ) and the probability ratio of the transitions is inversely related to the corresponding decay times, which give  $A = \tau_{21nr} / (\tau_{21nr} + \tau_{20nr})$ ,  $B = \tau_{20nr} / (\tau_{21nr} + \tau_{20nr})$ ,  $C = \tau_{10nr} / (\tau_{10nr} + \tau_{10r})$  and  $D = \tau_{10r} / (\tau_{10nr} + \tau_{10r})$ . See Fig. for the computational flowchart of the proposed algorithm.

For the sake of validation, the present method is applied to a photonic crystal (PC) constructed by triangular arrangement of polystyrene spheres of 500 nm diameter, which is placed on a 200 nm thick silver slab to form an HPPS (Fig.3 inset). The capability of this structure in producing a coherent light from fluorescent spontaneous emissions was previously reported by Shi et al. [28]. To the best of authors' knowledge, this is one of the most prominent publication addressing the coherence of fluorescence emission. In this case, the fluorescent material, fluorophore-doped polyvinil alcohol (PVA), forms a 50 nm thick layer on top of the HPPS and also fills the vacancy between spheres. In order to keep the numerical test-case substantially similar to the reported experimental setup, all parameters of the fluorophores, e.g. decay time constants, emission frequency, and excitation frequency, are set according to the physical attributes of Sulforhodamine 101 (S101).

In order to estimate the degree of temporal coherence, two different approaches has been employed; in one approach, the temporal coherence function (TCF) is utilized, which is the auto correlation of the signal,  $\Gamma(\tau) = \langle u(t+\tau)u^*(t) \rangle$ , where angle brackets and superscript \* denote the time averaging and complex conjugate, respectively. Here,  $u(t)$  is the electric field. The degree of coherence is conclusively determined as  $\gamma(\tau) = \Gamma(\tau)/\Gamma(0)$  and thus, the coherence time is  $\tau_c = \int_{-\infty}^{\infty} |\gamma(\tau)|^2 d\tau$  [41]. Using this

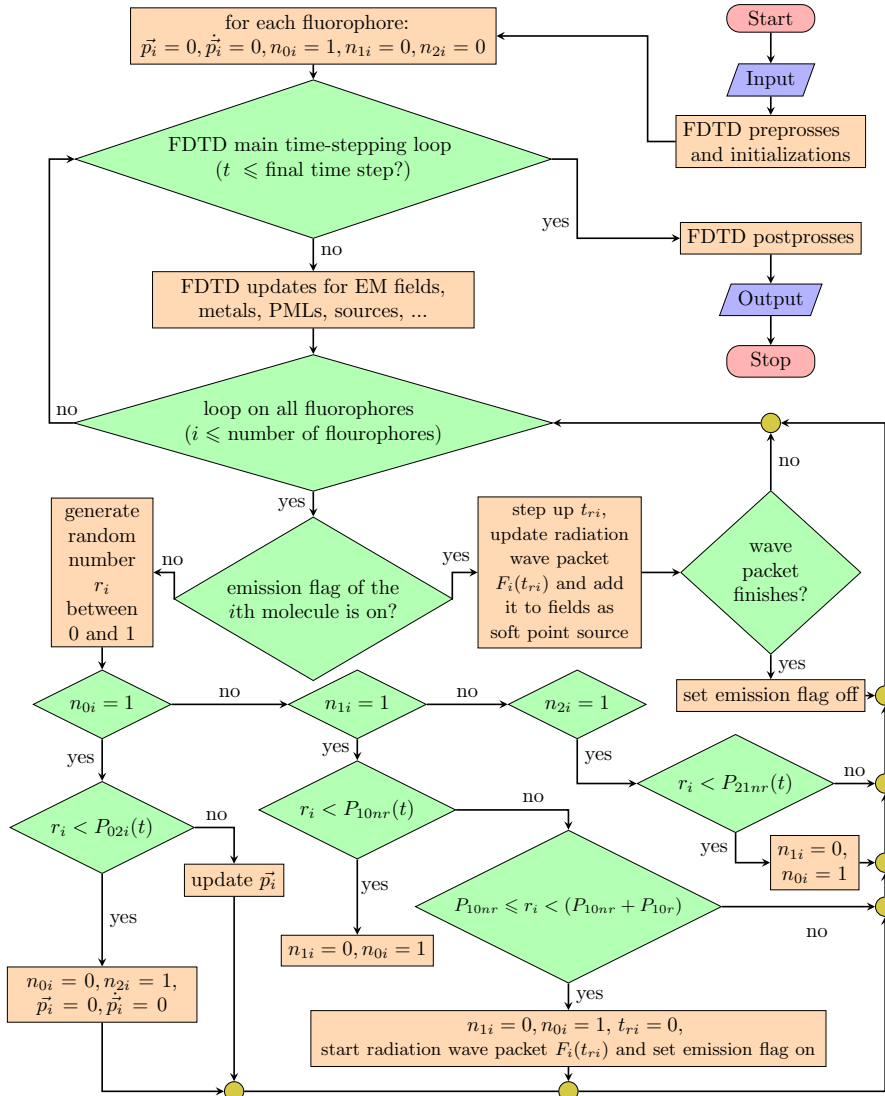


**Figure 2** The algorithm proposed for the implementation of the fluorescence effect within FDTD. In every FDTD time step, emission flag of each fluorophore (e.g. the  $i$ th one) is checked and if it is on, the emission continued. If the flag is off, the state of molecule should be checked. In case the molecule is at the ground state, an already randomly generated number,  $r_i$ , is compared to the absorption probability  $P_{02i}(t)$  and consequently either the transition to level 2 could take place or the dipole moment of the fluorophore should be updated. Likewise, in other cases (i.e. molecule is in the level 1 or 2) the same procedure should be followed with the respective probabilities.

approach for the present test-case, the coherence time is  $\tau_c = 1.14 \times 10^{-13}$  sec, this is approximately equivalent to the wavelength bandwidth of  $|\Delta\lambda| = 6.8$  nm. In the other approach, the desirable wavelength spectrum is obtained using the Fourier transform of the time-varying electric field. For the present test-case, this spectrum is shown in Fig.3. By fitting a Gaussian function into the figure, the emission bandwidth, i.e., the full-width at half-maximum (FWHM) of the peak is calculated to be approximately  $|\Delta\lambda| = 6.4$  nm.

It must be noted that in the present work, a perfectly ordered structure is modeled while any experimental test is subject to fabrication defects. These structural defects lead to a wider bandwidth and therefore, a lower tempo-

ral coherence can be detected for the experimental setup. This is due to the fact that any defect/disorder perturbs the Hamiltonian of the structure, which in turn broadens the band of energy [42]. Considering this issue, there is a good agreement between the result obtained using the proposed numerical method and that reported in the literature [28].

On the other hand, the most reliable and extremely practical approach to the estimation of spatial coherence is the Young double slits technique [43] for which, the interference fringe visibility as a function of the separation distance between slits is  $\mathcal{V}_{ij} = \frac{2\sqrt{u_i^2(t)u_j^2(t)}}{u_i^2(t)+u_j^2(t)} M_{ij}$  [41]. In this equation,

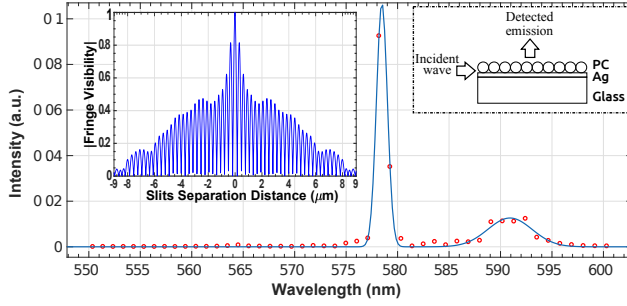


**Figure 3** Wavelength spectrum of reflection obtained using the proposed numerical method for the structure previously studied by Shi et al. [28]. The pick corresponds to the unabsorbed portion of the excitation wave is observed at  $\lambda = 578$  nm and the emission pick occurs at  $\lambda = 591$  nm. Shown in the right inset is the schematic of the structure while the fringe visibility as a result of the numerical modeling of the double-slits test is presented in the left inset.

$$M_{ij} = \frac{\langle u_i(t)u_j^*(t) \rangle}{\sqrt{\langle u_i^2(t) \rangle \langle u_j^2(t) \rangle}}$$

is the mutual coherence function between electric fields  $u_i(t)$  and  $u_j(t)$  detected at two distinct points  $i$  and  $j$  placed on a plane perpendicular to the direction of detection, which represent the positions of the slits. For the present test-case, the fringe visibility is plotted in the inset of Fig. 3. It is evident that visibility significantly decreases as the slits separation distance increases beyond  $4 \mu\text{m}$  and practically, no interference pattern can be observed for a separation distance of larger than  $8 \mu\text{m}$ . This is in close agreement with the result reported in the reference [28]. Nevertheless, it is noteworthy that using numerical simulation, it can be observed (in the inset of Fig.3) how the fringe visibility varies for a wide range of separation distances.

The above statements apparently confirm the validity of results obtained by the proposed numerical method and clearly shows its excellent performance on simulating the interaction between EM field and fluorescence. Anyhow, this numerical method facilitates studying the statistical characteristics of an ensemble of fluorophores, which is essential for advancements in the field of fluorescence coherence.

Here, the proposed method is applied to a novel HPPS that is constructed by placing an inverse photonic crystal, made by pore-opened [44] anodic aluminum oxide (AAO), on top of a 200 nm thick silver (Ag) layer (Fig.4). The cylindrical holes of PC are filled with S101-doped PVA, which also forms a layer of 50 nm thickness on top of the AAO. The structural parameters, i.e., thickness of AAO layer  $h = 500$  nm, diameter of cylindrical holes  $d = 200$  nm, and the center-to-center distance the neighboring cylinders  $a = 250$  nm, have been set in a way that not only the structure can be easily fabricated, but also, it significantly enhances the coherence as seen in the rest of this paper.

Similar to the previous test-case, the proposed HPPS experiences an incident continuous EM wave with a wavelength of 575 nm from its side that is perpendicular to the  $y$ -axis (Fig. 4) and the resulting vertical emission (along  $z$ -axis) is recorded. In this way, the detected wave would not be masked by the incident wave. Moreover, this is a wise

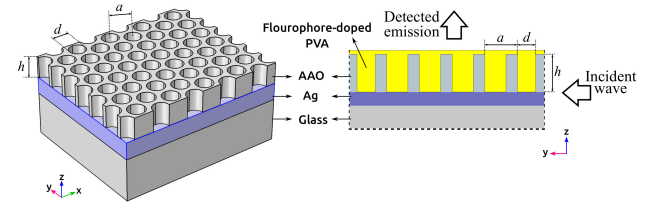


**Figure 4** The overall 3D view of the proposed hybrid anodic structure (left) and its  $yz$  cross-section (right).

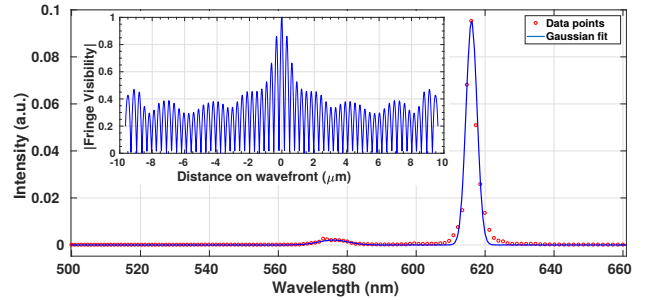


**Figure 5** Wavelength spectrum of the detected wave obtained for the proposed HPPS. The emission pick is observed at  $\lambda = 616$  nm, while a lower pick occurs at  $\lambda = 575$  nm that corresponds to the unabsorbed portion of the excitation wave. Shown in the inset is the fringe visibility as a function of the separation distance of the double-slits.

choice of the excitation and detection, which is appropriate for imaging and LED applications. In Fig. 5, the recorded field is shown in frequency domain. The graph hits its peak at  $\lambda = 616$  nm with a FWHM of  $|\Delta\lambda| = 3$  nm. On the other hand, using TCF, a coherence time of  $\tau_c = 2.1 \times 10^{-13}$  sec or equivalently  $|\Delta\lambda| = 4$  nm is calculated. It is observed that the presence of the proposed HPPS leads to an almost eight times greater coherence length for the fluorescence emission.

In order to identify the underlying cause of the emergence of such a narrow emission bandwidth, all modes propagated horizontally (along the  $xz$  plane) in PC of the proposed HPPS are also calculated and shown in Fig. 6. It is known that there is no possibility for p-polarized modes to be vertically propagated since the associated electric field is aligned with  $z$ -axis. On the other hand the electrical field is directed horizontally for s-polarized modes and thus, for each wavelength that the horizontal propagation is prevented by HPPS, a vertical reflection is possible. Therefore, considering that the excitation input wave is aligned with  $y$ -axis, one should focus on the  $y$ -directed s-polarized propagation graph in Fig. 6, which reveals a trough at  $\lambda = 616$  nm. In this sense, the portion of the emission band of S101 molecules that coincides with this trough is expected to reflect vertically while the rest propagates along the metal surface. Since for S101 molecules, the excitation band overlaps partially with the emission band, the horizontally propagated modes can excite the neighboring fluorophores. This synchronizes the transitions of the molecules and therefore, a



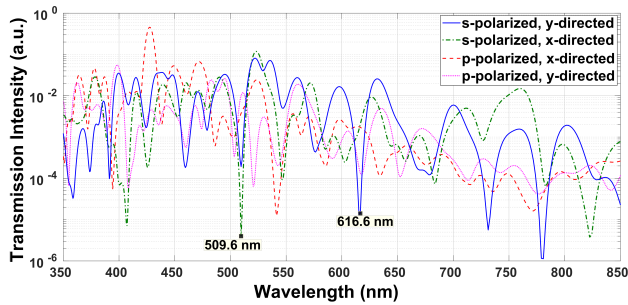


**Figure 6** Wavelength spectrum of horizontally propagated modes in PC of the proposed HPPS obtained for different directions of propagation in  $xy$ -plane with either s- or p-polarizations.

spatial coherence is also expected. The visibilities obtained as results of the double-slits tests are shown in Fig. 5 (inset), which clearly shows a spatial coherence width of greater than  $10\ \mu\text{m}$ . Anyway, this coherence width is proportional to the propagation length of the horizontally propagated modes, which is determined by the imaginary part of the corresponding wave-vectors. It can state that in the near-field, the plasmonic modes are responsible for coherence while the s-polarized modes are capable to transfer this coherence to the far-field. It must also be noted that the conversion between the s- and p-polarized modes is possible due to the random orientation of the dipole moment of the molecules and internal reflections inside cavities. It is worth noting that the wider the spectral range of the horizontally propagated modes, the larger the portion of energy absorbed by structure. This is the case for the proposed HPPS as seen in Fig. 6, where only a small portion of modes (corresponding to the troughs) is prevented from being horizontally propagated, and thus, a large portion of the incident energy is responsible for exciting the fluorophores (see Fig. 5). This is also among desirable features of the proposed HPPS compared to the previously proposed structures.

The peaks and troughs of the reflection graphs can be shifted by slightly changing the structural parameters of HPPS. In this way, the proposed HPPS can be adjusted to achieve coherence for different fluorophores. Moreover, comparing to the colloidal structure, the proposed HPPS benefits from a more robust structure and can more easily be fabricated with a lower cost, while resulted in significantly enhanced temporal and spatial coherence. Another point is that a colloidal structure with spherical cavities causes leaky modes with no preferred direction and therefore, as expected, smoother wavefronts are observed for the proposed structure with vertically aligned cavities (cylinders). An interesting but still open topic is the phase transition from incoherence to coherence, which necessarily requires to study a wide range of parameters. Numerical simulation can provide an efficient means for such a study by considerably alleviating the costs associated with experiments. Anyhow, to the best of authors' knowledge, the proposed numerical algorithm is the only one capable of handling this class of simulations.

## References

- [1] V. I. Shcheslavskiy, M. V. Shirmanova, V. V. Dudenkova, K. A. Lukyanov, A. I. Gavrina, A. V. Shumilova, E. Zagaynova, and W. Becker, *Opt. Lett.* **43**(13), 3152–3155 (2018).
- [2] D. A. Giljohann and C. A. Mirkin, *Nature* **462**(7272), 461–464 (2009).
- [3] T. Ribeiro, C. Baleizão, and J. P. S. Farinha, *Scientific Reports* **7** (2017).
- [4] R. J. Moerland, L. Eguiluz, and M. Kaivola, *Optics express* **21**(4), 4578–4590 (2013).
- [5] T. Zhao, K. Yu, L. Li, T. Zhang, Z. Guan, N. Gao, P. Yuan, S. Li, S. Q. Yao, Q. H. Xu et al., *ACS applied materials & interfaces* **6**(4), 2700–2708 (2014).
- [6] L. Wang, Q. Song, Q. Liu, D. He, and J. Ouyang, *Advanced Functional Materials* **25**(45), 7017–7027 (2015).
- [7] M. Bauch, K. Toma, M. Toma, Q. Zhang, and J. Dostalek, *Plasmonics* **9**(4), 781–799 (2014).
- [8] M. K. Kwon, J. Y. Kim, B. H. Kim, I. K. Park, C. Y. Cho, C. C. Byeon, and S. J. Park, *Advanced Materials* **20**(7), 1253–1257 (2008).
- [9] A. Kinkhabwala, Z. Yu, S. Fan, Y. Avlasevich, K. Müllen, and W. Moerner, *Nature Photonics* **3**(11), 654–657 (2009).
- [10] H. Aouani, O. Mahboub, E. Devaux, H. Rigneault, T. W. Ebbesen, and J. Wenger, *Nano letters* **11**(6), 2400–2406 (2011).
- [11] G. Lozano, D. J. Louwers, S. R. Rodríguez, S. Murai, O. T. Jansen, M. A. Verschuuren, and J. G. Rivas, *Light: Science & Applications* **2**(5), e66 (2013).
- [12] L. Langguth, D. Punj, J. Wenger, and A. F. Koenderink, *ACS nano* **7**(10), 8840–8848 (2013).
- [13] P. Anger, P. Bharadwaj, and L. Novotny, *Physical review letters* **96**(11), 113002 (2006).
- [14] T. Pons, I. L. Medintz, K. E. Sapsford, S. Higashiya, A. F. Grimes, D. S. English, and H. Mattoussi, *Nano letters* **7**(10), 3157–3164 (2007).
- [15] X. Li, J. Qian, L. Jiang, and S. He, *Applied Physics Letters* **94**(6), 063111 (2009).
- [16] P. Reineck, D. Gómez, S. H. Ng, M. Karg, T. Bell, P. Mulvaney, and U. Bach, *ACS nano* **7**(8), 6636–6648 (2013).
- [17] S. G. Romanov, A. V. Korovin, A. Regensburger, and U. Peschel, *Advanced Materials* **23**(22-23), 2515–2533 (2011).
- [18] X. Yang, A. Ishikawa, X. Yin, and X. Zhang, *ACS Nano* **5**(4), 2831–2838 (2011).
- [19] Z. Zhang, L. Zhang, M. N. Hedhili, H. Zhang, and P. Wang, *Nano letters* **13**(1), 14–20 (2012).
- [20] A. H. Schokker, F. van Riggelen, Y. Hadad, A. Alù, and A. F. Koenderink, *Physical Review B* **95**(8), 085409 (2017).
- [21] X. Zhu, F. Xie, L. Shi, X. Liu, N. A. Mortensen, S. Xiao, J. Zi, and W. Choy, *Optics letters* **37**(11), 2037–2039 (2012).
- [22] M. López-García, J. F. Galisteo-López, A. Blanco, J. Sánchez-Marcos, C. López, and A. García-Martín, *small* **6**(16), 1757–1761 (2010).
- [23] B. Ding, C. Hrelescu, N. Arnold, G. Isic, and T. A. Klar, *Nano letters* **13**(2), 378–386 (2013).
- [24] S. B. Raghunathan, H. F. Schouten, and T. D. Visser, *Optics letters* **37**(20), 4179–4181 (2012).
- [25] J. J. Greffet, R. Carminati, K. Joulain, J. P. Mulet, S. Mainy, and Y. Chen, *Nature* **416**(6876), 61–64 (2002).

- [26] M. De Zoysa, T. Asano, K. Mochizuki, A. Oskooi, T. Inoue, and S. Noda, *Nature Photonics* **6**(8), 535–539 (2012).
- [27] L. Shi, T. Hakala, H. Rekola, J. P. Martikainen, R. Moerland, and P. Törmä, *Physical review letters* **112**(15), 153002 (2014).
- [28] L. Shi, X. Yuan, Y. Zhang, T. Hakala, S. Yin, D. Han, X. Zhu, B. Zhang, X. Liu, P. Törmä et al., *Laser & photonics reviews* **8**(5), 717–725 (2014).
- [29] M. Bradford and J. T. Shen, *Opt. Lett.* **39**(19), 5558–5561 (2014).
- [30] S. Y. Lee and M. A. Mycek, *Opt. Lett.* **43**(16), 3846–3849 (2018).
- [31] J. Lee and J. M. Kosterlitz, *Phys. Rev. Lett.* **65**(Jul), 137–140 (1990).
- [32] T. Schwartz, G. Bartal, S. Fishman, and M. Segev, *Nature* **446**(7131), 52 (2007).
- [33] S. J. Tan, M. J. Campolongo, D. Luo, and W. Cheng, *Nature nanotechnology* **6**(5), 268 (2011).
- [34] M. Sani and M. H. Farzad, *Physical Review B* **97**(8), 085406 (2018).
- [35] P. Genevet, J. P. Tetienne, E. Gatzogiannis, R. Blanchard, M. A. Kats, M. O. Scully, and F. Capasso, *Nano Letters* **10**(12), 4880–4883 (2010).
- [36] D. Wang, T. Yang, and K. B. Crozier, *Optics express* **19**(3), 2148–2157 (2011).
- [37] M. Bauch and J. Dostalek, *Optics express* **21**(17), 20470–20483 (2013).
- [38] A. Taflove and S. C. Hagness, *Computational electrodynamics: the finite-difference time-domain method* (Artech house, 2005).
- [39] A. Jablonski, *Nature* **131**(839-840), 21 (1933).
- [40] J. R. Albani, *Principles and applications of fluorescence spectroscopy* (John Wiley & Sons, 2008).
- [41] J. W. Goodman, *Statistical optics* (John Wiley & Sons, 2015).
- [42] I. Mukherjee and R. Gordon, *Opt. Express* **20**(15), 16992–17000 (2012).
- [43] W. Martienssen and E. Spiller, *American Journal of Physics* **32**(12), 919–926 (1964).
- [44] L. Bruschi, G. Mistura, P. T. M. Nguyen, D. D. Do, D. Nicholson, S. J. Park, and W. Lee, *Nanoscale* **7**, 2587–2596 (2015).